

Banner appropriate to article type will appear here in typeset article

# Regular reflection to Mach reflection (RR-MR) transition in Short wedges

Vinod Yeldho Baby<sup>1</sup> †, Vinoth Paramanandham<sup>1</sup> and G. Rajesh<sup>1</sup>

<sup>1</sup>Indian institute of Technology Madras, Chennai, India.

(Received xx; revised xx; accepted xx)

Regular reflection (RR) to Mach reflection (MR) transitions (RR $\leftrightarrow$ MR) on long wedges in steady supersonic flows have been well studied and documented. However, in a short wedge where the wedge length is small, the transition prediction becomes really challenging owing to the interaction of the expansion fan emanating from the trailing edge of the wedge with the incident shock and the triple/reflection point. The extent of this interaction depends on the distance between the wedge trailing edge and the symmetry line ( $H_t$ ). This distance is a geometric combination of the distance of the wedge leading edge from the symmetry line ( $H$ ), the wedge angle ( $\theta$ ), and the wedge length ( $w$ ). In the present work, the RR $\leftrightarrow$ MR transitions have been studied using analytical and computational methods, and the transition lines are plotted for various Mach numbers and wedge lengths. The transition criterion strongly depends on the wedge length, which can be so adjusted to eliminate the RR $\leftrightarrow$ MR transitions till the wedge angle reaches the no-reflection domain.

## 1. Introduction

When a supersonic flow passes over symmetric wedges, the flow turning results in a shock interaction/reflection. Depending on the flow parameters, the reflection can be either a Mach reflection (MR) or a regular reflection (RR). The possible shock reflections between the maximum and minimum  $H_t$  values, as shown in figure 1, have been investigated extensively (Li & Ben-Dor 1997). The  $H_t$  value depends on the wedge length  $w$ , wedge angle ( $\theta$ ) and the center line distance  $H$  of the wedge leading edge, as shown in figure 1 (a) and (b). Based on the  $w/H$  ratio, we may classify the wedges into long and short wedges. In long wedges, the expansion fan from the trailing edge of the wedge does not interact with the incident shock from the leading edge of the wedge, as shown in figure 2. Short wedges have a  $w/H$  ratio small enough to have the expansion fan interacting with the incident shock wave and triple/ reflection point as shown in figure 3. Due to the expansion fan interaction, the incident shock angle is continuously reduced from the point where the leading expansion characteristic meets the shock to the triple/reflection point. This progressive reduction in the shock angle curves the incident shock as it approaches the triple/reflection point. The curvature of the incident shock essentially depends on the extent of the expansion fan interaction, which in turn, depends on the wedge length ( $w$ ), the distance between the leading edge and line of symmetry ( $H$ ) or the  $w/H$  ratio and the wedge angle ( $\theta$ ) as shown in Fig.3. Thus, the shock

† Email address for correspondence: ae20d001@smail.iitm.ac.in

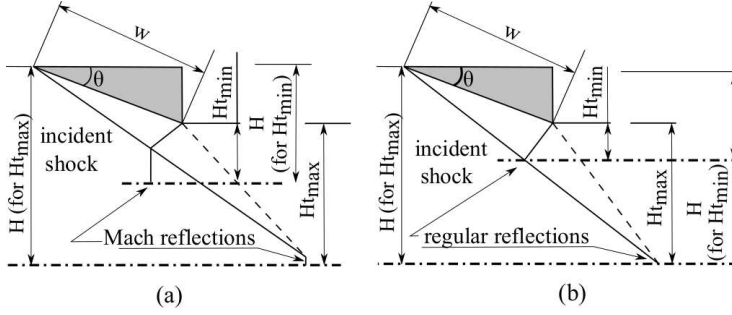


Figure 1:  $H_{t,min}$  and  $H_{t,max}$  for (a) MR and (b) RR.

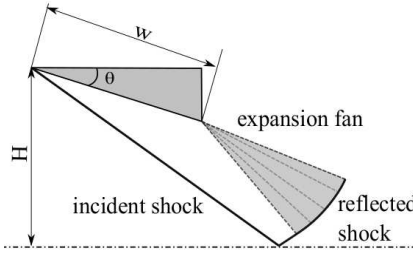


Figure 2: Long wedge.

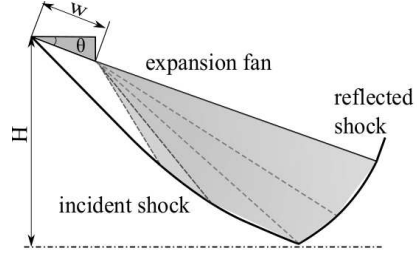


Figure 3: Short wedge.

angle at the reflection point for a short wedge will depend not only on the wedge angle and the flow Mach number but also on the  $w/H$  ratio. Any attempts to predict the shock transitions on short wedges should necessarily model the incident shock curvature due to its interaction with the expansion fan accurately.

### 1.1. Previous works in Shockwave- Expansion fan Interaction

The interactions of shock waves and expansion waves in one-dimensional flows are the subject of several investigations, especially in the inlet designs of high-speed flows (Clarke 2002). A comprehensive description of the interactions of shock waves, expansion waves and contact surfaces, mainly in shock tube flows, can be seen in the monograph by Glass (1991). One of the early works in expansion fan shock wave interaction in symmetric wedge flows was carried out by Li & Ben-Dor (1996) in which an analytical solution was obtained for the curvature of the shock wave due to its interaction with a centered expansion wave of the opposite family. The curvature of the shock wave was approximated as a second-order polynomial. In the experimental and numerical validations of this analytical model (Nel *et al.* 2015), it was found that though the model prediction was accurate for small interactions, it could not predict the shock curvature for the stronger interactions. In another study (Hillier 2007) on the shock-wave/expansion-wave interaction and the transition between regular and Mach reflections, analytical and numerical simulations were carried out to investigate the inviscid interactions of an expansion wave with an incident shock wave of the opposite family. The study was to stabilize a Mach reflection in a parallel duct for different flow conditions. It was observed that the stabilization could be achieved for a narrow range of Mach numbers and depends on the relative positions of the origin of shock wave and expansion wave. Most analytical methods developed in shock reflections focused on predicting the MR configuration and the Mach stem height, a finite length scale in an MR in long wedges (Azevedo & Liu 1993; Li & Ben-Dor 1997; Mouton & Hornung 2007). In these models, the slip line, which originates from the triple point in a Mach

Reflection, was assumed to be a straight line. Later, the refinement of the slip line curvature was carried out by (Bai & Wu 2017), resulting in a better Mach stem prediction, as they considered the expansion waves generated over the slip line and its interaction with the transmitted expansion waves through the reflected shock. Further, numerical studies of a shock reflection in the presence of an upstream expansion wave and a downstream shock wave for two-dimensional flows by (Yao *et al.* 2013) reported that found that the expansion fan delayed the RR↔MR transition at lower Mach numbers (Mach 2 – 3.5) and expedited it at higher Mach numbers.

The analytical models discussed above were all for the interaction of the shock wave with the opposite (either right running or left running) family of expansion waves. On the contrary, in short wedges the incident shock is curved due to the prolonged interaction of the expansion wave of the same family. The study of this type of interaction is significant since the RR↔MR transition may solely depend on the incident shock angle at the reflection point, which is determined by the shock curvature due to the interaction. It is hence, essential to determine the parameters governing the shock angle at the reflection point and the change in transition criteria when these parameters vary. No works have been reported till date to investigate the short wedge effects in the RR↔MR transitions and the MR configurations, to the best of the author's knowledge. In the present investigation, an analytical model is hence developed to study the prolonged interaction of an expansion wave with an incident shock wave of the same family to predict the shock wave curvature. This is used to investigate the shock transitions in symmetric short wedges. The analytical model is validated with an in-house inviscid, 2D, structured finite volume solver with a fifth-order WENO scheme. The RR↔MR transition lines are expected to be altered by the interactions of the expansion wave with the shock wave due to the small wedge lengths.

## 2. Shock wave expansion fan interaction - Analytical Modeling

The shock–expansion interaction is modeled with the method of characteristics (MoC). The model assumptions are that the flow is steady, compressible, inviscid, two-dimensional (planar), isentropic, and rotational as it is a curved shock. The entropy is constant only along the streamlines. The basic configuration of the incident shock-expansion fan interaction model is shown in figure 4. The characteristic and compatibility equations for two-dimensional, isentropic, rotational, and supersonic flow are given below in Table 1.

The initial value line for the MOC is the first characteristic expansion line from the trailing edge (point D), which terminates at the intersection of the incident shock wave and the first expansion line (point B). The solution algorithm is initiated by giving a small increment of flow turn angle downstream from point D. The flow properties are determined using the Prandtl-Meyer relations. The C– curve from point D and C+ curve from point B intersect at point B1. The flow properties and location at point B1 are obtained by solving the above-mentioned characteristic and compatibility equations from B and D. The curved shock is obtained by solving discrete points on the shock. Since MoC is not valid across the shock, the solution point at the shock curvature is obtained by iteratively computing the local pressure ratio across the shock. Post-shock properties are calculated with the local incoming Mach number and the assumed pressure ratio across the shock. These flow properties should satisfy the compatibility equation along the C- curve originating from the interior point B1. The iterations stop when this condition is satisfied. The local shock angle is obtained, and the x and y positions of the shock curvature is obtained by solving the characteristic equations. Subsequent points on the shock curvature are obtained by incrementing the next flow turn angle at point D and repeating the above steps. One of the algorithms calculates

---

**Characteristic Equations**


---

$$(dy/dx) = \lambda_0 = v/u \quad (\text{Streamline})$$

$$(dy/dx) = \lambda_+ = \tan(\alpha + \mu) \quad (\text{Right running characteristic line, '+' subscript})$$

$$(dy/dx) = \lambda_- = \tan(\alpha - \mu) \quad (\text{Left running characteristic line, '-' subscript})$$

**Compatibility Equations**


---

$$\rho V dV + d\rho = 0 \quad (\text{Streamline})$$

$$dp - a^2 d\rho = 0 \quad (\text{Streamline})$$

$$\frac{\sqrt{(M^2-1)}}{(\rho V^2)} dp_+ + d\alpha_+ = 0 \quad (\text{Right running characteristic Mach, '+' subscript})$$

$$\frac{\sqrt{(M^2-1)}}{(\rho V^2)} dp_- - d\alpha_- = 0 \quad (\text{Left running characteristic line, '-' subscript})$$

---

Table 1: Steady, two dimensional, isentropic, rotational supersonic flow

---

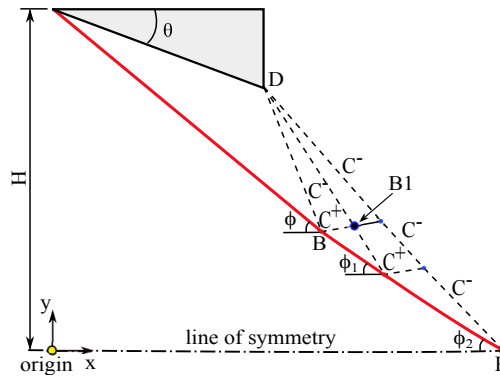


Figure 4: Shock-expansion fan interaction model using MoC.

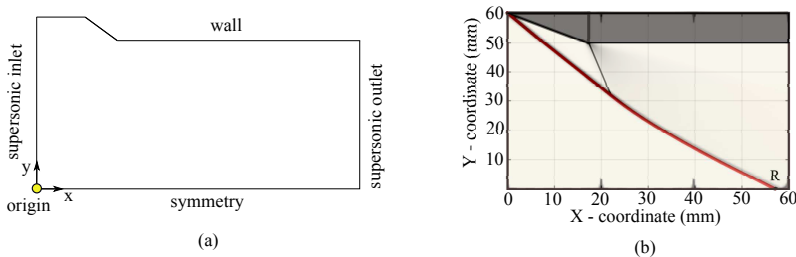


Figure 5: (a) CFD domain (b) Superimposed image of Analytical and computational result

the interior points in the flow field, while the other determines the discrete points along the shock curvature. The analytical model developed does not consider the possibility of Mach reflection and is valid only for regular reflection.

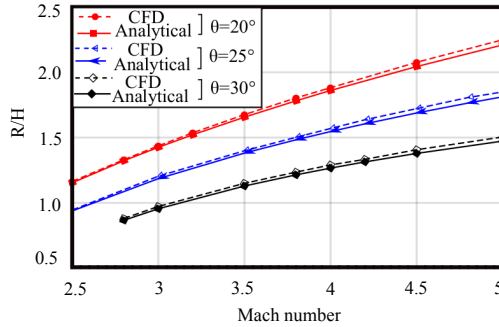


Figure 6: Validation curve for  $w/H=0.33$

### 3. Shockwave expansion fan interaction - CFD Modeling

The computational domain of the model is as shown in figure 5(a). The validation of the analytical model with CFD is carried out by superimposing the curved shock locus. The superimposed images of the analytical results and the computational results as shown in figure 5(b) reveal that the analytical prediction agrees very well with the CFD results qualitatively. The same is done by varying the Mach number,  $w/H$  ratio and the wedge angle. The Mach number vs the non-dimensional shock reflection distance [shown in figure 4] ( $R/H$ ) for different  $w/H$  ratios, obtained from analytical and CFD results are plotted. Figure 6 shows one such plot of Mach number vs  $R/H$  for the  $w/H$  ratio 0.33, for different wedge angles. It is seen that the maximum deviation between the analytical and CFD results are less than 2%.

## 4. Results and Discussion

The transition of the shock reflection in a short wedge depends on the extent of the interaction of the expansion fan with the incident shock wave. Due to the interaction of the expansion fan, the incident shock is weakened, resulting in a decrease in the shock angle at the reflection point compared to the case where there is no interaction. Therefore, the transition angle between RR and MR is modified. The value of the shock angle at the point of reflection depends on the degree of interaction of the expansion fan, or conversely, the  $w/H$  ratio, while  $M$  and  $\theta$  remain constant. As stated by Li & Ben-Dor (1997), the transition angle is typically determined using the detachment criterion for RR→MR or the von Neumann criterion for MR→RR. In the following sections, we will quantify the transition angles for the short wedges for various  $w/H$  ratios using the MOC method described in section 2 and validate these results with higher-order numerical simulations. In addition, based on the  $w/H$  ratios, we have categorized the various processes in the transition angles into three distinct types.

### 4.1. Transition curves- Detachment criterion validation

The delay in the transition criterion, specifically the detachment condition within the short wedge, can be attributed to the attenuation of the incident shockwave. The extent of the delay of this transition is determined by the  $w/H$  ratio. The determination of the detachment condition involves the solution of MOC for a specified Mach number ( $M$ ), wedge angle ( $\theta$ ), and  $w/H$ . The detachment condition is generally shifted to higher wedge angles for the shorter wedges, and it is constrained by the no-reflection domain. Figure 7 shows the shift in the detachment criterion for a  $w/H$  ratio of 0.5. The blue line represents the modified detachment criterion resulting from the interaction of the expansion fan with the incident shockwave, whereas the black solid line represents the detachment condition for long wedges

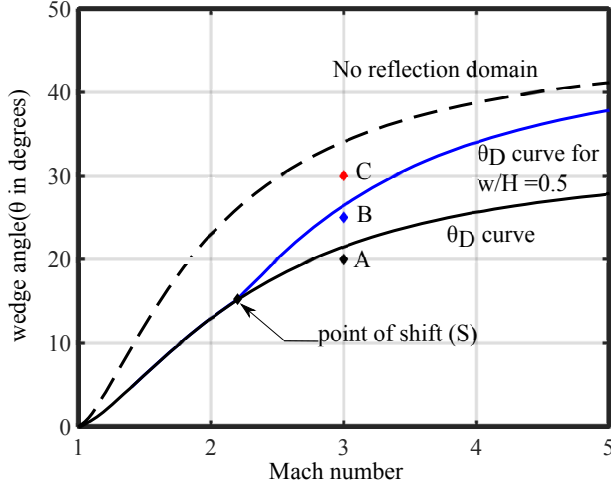


Figure 7: (a) Transition lines - Shift in Detachment criteria for  $w/H = 0.5$ .

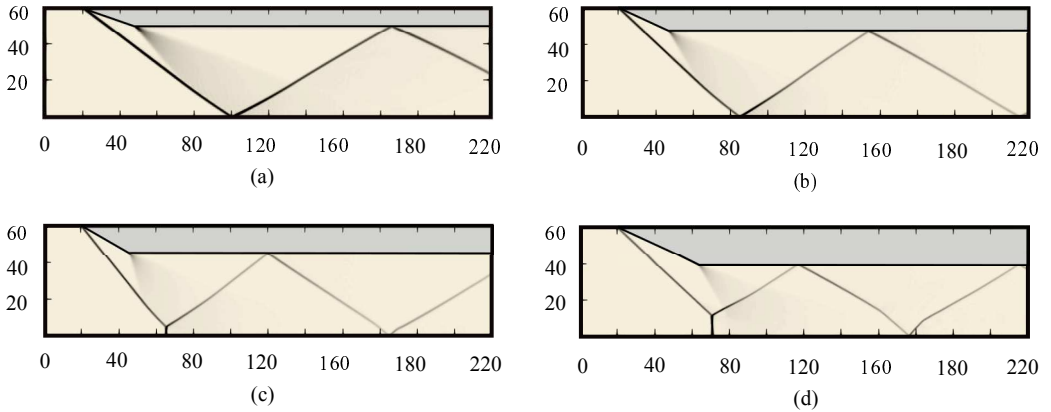


Figure 8: (a) Flow configurations corresponding to points A, (b) B, (c) C (all short wedges) and (d) case without interaction(long wedge), where  $M=3$ ,  $w/H = 0.5$  and  $\theta = 20^\circ, 25^\circ, 30^\circ$  respectively for short wedges and,  $M=3$ ,  $w/H = 0.81$  and  $25^\circ$  for long wedge.

in the absence of expansion fan interaction. The transition line obtained from the MOC is validated with numerical simulations for  $M = 3$  flow over a supersonic wedge; three cases are considered by keeping the Mach number constant and varying the wedge angle to comprehend the type of reflection obtained from the numerical simulations. The wedge angles are set to  $\theta_w = 20^\circ, 25^\circ, 30^\circ$  respectively (points A, B, and C in Figure 7), and  $w/H$  is set to 0.5 (short wedge case) and 0.81 (long wedge case). Figure 8a-d depicts the numerical schlieren for the simulation of the short wedge at points A, B, and C and the simulation of the long wedge at point B. As shown in Figure 8a-c, the results for the shorter wedge correspond to the MOC results by displaying the RR configuration for points A and B and transforming to MR for point C. Point B in Figure 8d depicts an MR configuration for the long wedge case.

Point S in Figure 7 depicts the beginning of the interaction between the expansion fan and the incident shock wave for a given  $w/H$  ratio. The deviation of the detachment condition occurs after this value, and for values below the interaction point, it remains the same as

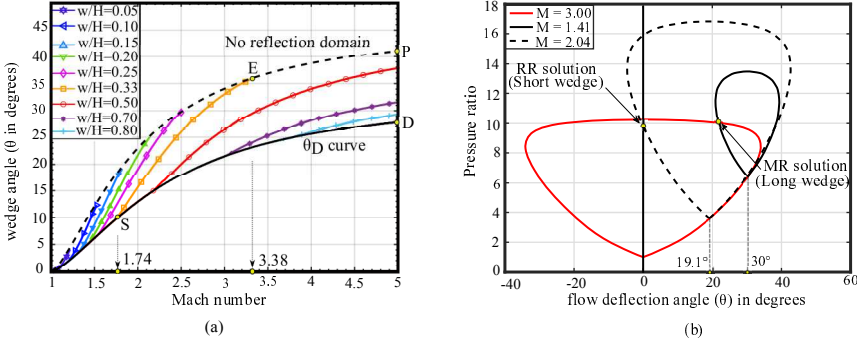


Figure 9: (a) Transition lines - Shift in Detachment criterion for various  $w/H$  ratio.(b) Shock polar representation for  $w/H = 0.33$

the long wedge. Figure 9 demonstrates that for all  $w/H$  ratios, there exists a combination of  $M$ - $\theta$  for which the interaction begins, and the transition line shifts from that point. Figure 9 shows that  $w/H = 0.33$  begins to deviate from the detachment condition line when  $M = 1.74$  and  $\theta_w = 9.6^\circ$ . The shift ends at the no-reflection condition corresponding to  $M = 3.38$  and  $\theta_w = 36.3^\circ$ . For  $w/H = 0.33$ , the region under the curve SEPD will be RR, which eliminates MR flow configurations for any combination of Mach number and wedge angle beyond point E, as illustrated in Figure 9. Thus, the development of transition conditions for a shorter wedge has far-reaching implications in that one can select a domain in which only a specific type of reflection occurs or control the size of the Mach reflection configuration by adjusting the  $w/H$  ratio.

#### 4.2. Shock polar representation of the Interaction effects

Figure 10 depicts the polar shock representation of a long and short wedge with a  $w/H$  ratio of 0.33. The incoming flow has a Mach number of 3 and a wedge angle of 30 degrees. The incident polar (i-polar) for  $M=3$  is depicted as a red line, along with the reflected polars (r-polar) for the long wedge (solid black line) and short wedge (dashed black line). At the reflection point, the post-shock Mach number for a long wedge is 1.41, while it is 2.04 for a short wedge. The shock polar yields the MR solution corresponding to the long wedge and the RR solution corresponding to the short wedge. The shock polar reveals that the expansion fan interaction decreases the required flow turn angle at the reflection point in short wedges, even though the wedge angle remains unchanged.

#### 4.3. Dual solution domain in short wedges

Another significant transition line in the wedge flows is the von Neumann criterion. Intuitively, it makes sense to assume that as the  $w/H$  ratio decreases, the von Neumann criterion shifts towards higher wedge angles, similar to the detachment condition. The region between the detachment criterion line and the von Neumann criterion line, the dual solution domain, also undergoes this shift. In order to comprehend the change in the dual solution domain, transition lines for the von Neumann criterion were also drawn for various  $w/H$  ratios. The von Neumann criterion line for the short wedge is more complex than the detachment criterion, and the dual solution domain can be subdivided into three types based on the location of the bifurcation point. In the type I domain, the bifurcation point is identical to the long wedge flows, and the von Neumann criterion follows the long wedge von Neumann transition line prior to expansion fan interaction, shifting to higher wedge angles once expansion fan interaction commences. In the type II domain, the detachment criterion line deviates before

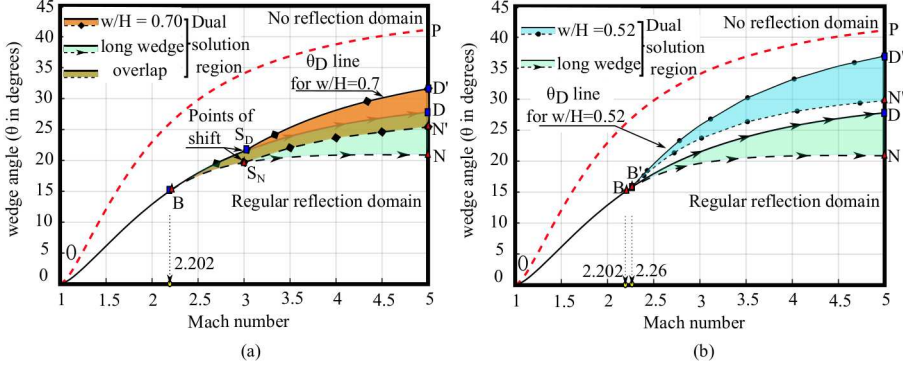


Figure 10: Dual solution domains for short wedges for different  $w/H$  ratios (a)  $w/H=0.7$  and long wedge and (b)  $w/H=0.52$  and long wedge

the von Neumann condition for long wedges, while the bifurcation point shifts from analytical solutions of mechanical equilibrium conditions for long wedges and follows the detachment criterion line for short wedges. For the type III domain, neither the von Neuman nor the dual domain solution exists, indicating that the flow field is RR across the entire parameter space. In the following sections, the three types of domains will be discussed.

#### 4.3.1. Type I Dual solution domain

The dual solution domain of type I is similar to the dual solution domain of the long wedges, with the same bifurcation point for the von Neumann line. This indicates that the transition line follows the long wedges prior to the expansion fan interaction and shifts to higher angles once the interaction begins. The von Neumann criterion ( $\theta_N$ ) line and detachment criterion ( $\theta_D$ ) line for  $w/H$  ratio 0.7 is shown in Figure 10 (a). For long wedges, the path  $OBS_D D$  and  $OBS_N N$  represents the  $\theta_D$  and  $\theta_N$  lines. B is the bifurcation point, and the dual solution domain begins. Both the transition lines follow the same path as that for a long wedge, up to the points of shift ( $S_D$  and  $S_N$  for the detachment line and von Neumann line, respectively), then follow a different path as ( $S_D - D'$  and  $S_N - N'$ ). For a short wedge, the path  $OBS_D D'$  and  $OBS_N N'$  represents the  $\theta_D$  and  $\theta_N$  line. The point of the shift of the  $\theta_D$  line is at point  $S_D$ , where  $M=3.03$  and wedge angle  $\theta = 21.66^\circ$ , whereas the point of the shift of the  $\theta_N$  line is at point  $S_N$ , where  $M=3$  and wedge angle  $\theta = 19.66^\circ$ . As the  $w/H$  value decreases from 0.7, the point of shifts  $S_D$  and  $S_N$  moves to the direction of the bifurcation point B, and at  $w/H=0.52$ , merges with the bifurcation point B', where  $M = 2.26$  and  $\theta_W = 15.75^\circ$  as shown in figure 10(b). It is worth noting that when the  $w/H$  ratio is decreased from 0.7 to 0.52, the bifurcation point shifts from B to B'. Thus, for all wedges with  $w/H$  ratios greater than 0.52, the bifurcation point B will remain the same since both the detachment line shift ( $S_D$ ) and von Neumann line shift ( $S_N$ ) occur after the bifurcation point B.

#### 4.3.2. Type II Dual solution domain

As illustrated in Figure 10 (b), the type II dual solution domain occurs when the detachment condition deviation occurs prior to the bifurcation point B' for  $w/H$  ratios less than 0.52. Consequently, the type II domain begins at  $w/H = 0.52$  and ends at  $w/H = 0.25$ . The dual solution domains for  $w/H$  ratios 0.25, 0.33, 0.5, 0.7, and long wedge are shown in Figure 11. In the figure, for the long wedges, paths  $OBD$  and  $OBN$  represent the  $\theta_D$  and  $\theta_N$  lines, respectively. Paths  $OB'D'_{(0.5)}$  and  $OB'N'_{(0.5)}$  represent the same for a short wedge of  $w/H$  ratio 0.5, and the bifurcation point shifted from B to point B', where  $M=2.258$  and wedge

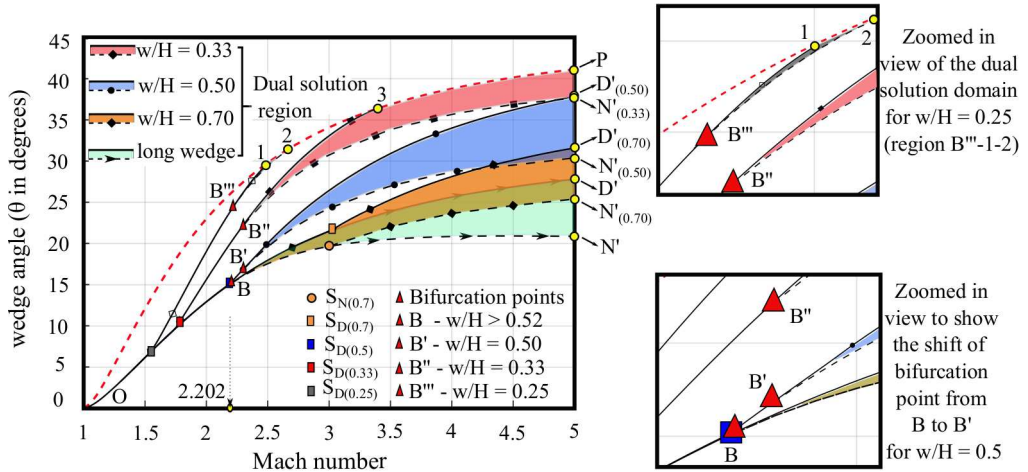


Figure 11: Dual solution domains for long and short wedges

angle  $\theta = 16.15^\circ$ . It is interesting to notice that for the case of the  $\theta_D$  line, the point of shift always occurred from the existing detachment line drawn for long wedges. In the presence of a strong expansion fan interaction, the bifurcation point shifts away from its original location, significantly modifying the dual solution domain. For a short wedge of much smaller  $w/H$  ratio 0.33, the  $\theta_D$  line and  $\theta_N$  line follow the path  $OB''P$  and  $OB''N'_{(0.33)}$  respectively as shown in Figure 11. The detachment criterion line intersects the no-reflection line at point 3 and then follows the no-reflection line. A major part of the dual solution domain is between the no reflection line and the  $\theta_N$  line. As the  $w/H$  ratio decreases from 0.5 to 0.25, the bifurcation point shifts from B and moves towards the no-reflection region, as illustrated in Figure 11.

#### 4.3.3. Type III Dual solution domain

The type III domain differentiates itself from the other two domains since the von Neumann condition graces the detachment criterion line, and thus, virtually, there is no dual solution domain exists. For any  $w/H$  ratio below 0.25, the reflection pattern does not change from the RR configuration. For example, the  $\theta_D$  line for  $w/H$  ratio 0.25 is shown as path  $OB'''1$ , in which point  $S_{D(0.25)}$  is the point of the shift from  $\theta_D$  line, where  $M=1.55$  and  $\theta = 6.86^\circ$ . The bifurcation point is at point B''', where  $M=2.22$  and  $\theta = 24.47^\circ$ . From the bifurcation point, the  $\theta_N$  line graces the  $\theta_D$  line, and eventually, these two lines meet at the no-reflection line at points 1 and 2, respectively. Due to the close paths of the transition lines, the dual solution domain for  $w/H$  ratio 0.25 is hardly visible in the plot. The  $\theta_D$  line,  $\theta_N$  line, and the no reflection line appear to merge for  $w/H$  ratios less than 0.25. Thus, the dual solution domain does not appear to exist for  $w/H$  ratios less than 0.25.

#### 4.3.4. Locus of the Bifurcation Point

The shifting of the bifurcation point is the defining characteristic of short wedge flows. It is evident from the preceding discussion that for  $w/H$  ratios less than 0.52, the bifurcation point moves, and Figure 12 illustrates the location of the bifurcation point in the red dashed line for various  $w/H$  ratios. The region between the detachment line and the no-reflection line is divided into two distinct areas by the red dashed line. Dual-domain solutions do not exist on the left side of the locus of the bifurcation line, but they do exist on the right. Figure 12 also depicts the bifurcation point's nonlinear movement closer to the detachment and no-reflection lines. Away from these lines, the point of bifurcation in the  $M - \theta_W$  parameter

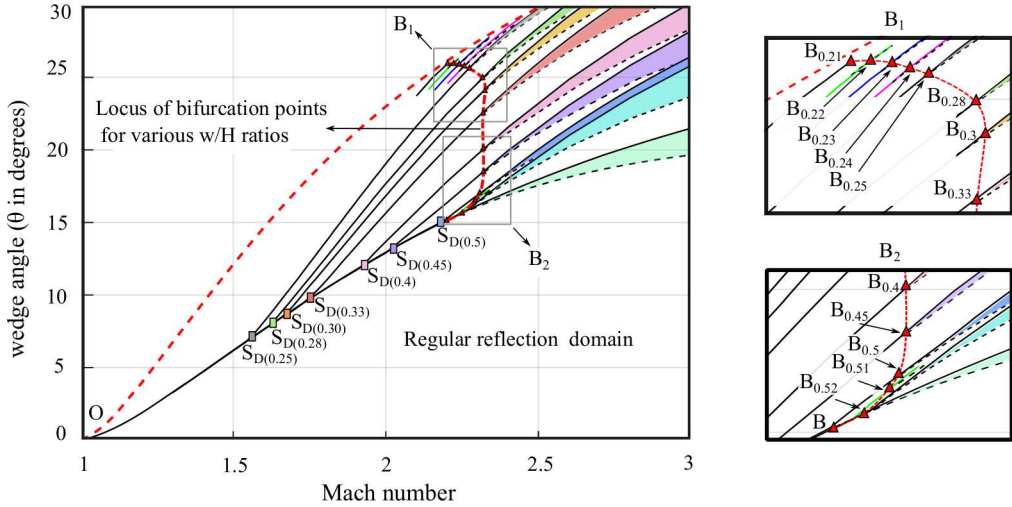


Figure 12: Locus of bifurcation points for various  $w/H$  ratio

space follows an almost straight line. The significance of the movement of the bifurcation point remains to be thoroughly studied and comprehended.

## 5. Conclusion

The shock reflection phenomena on short wedges have been investigated analytically and computationally. The interaction of the expansion fan emanating from the trailing edge of the short wedge with the incident shock wave is found to curve the incident shock. The curving of the incident shock wave leads to the change of shock angle at the reflection/triple point, consequently leading to a shift in the transition line. The transition lines plotted for different  $w/H$  ratios from 0.05 to 0.8 show that the shift in transition lines depends on the extent of interaction. The plot is useful in finding the detachment/von Neumann criterion for any Mach number between 1 and 5 for a particular  $w/H$  ratio. Moreover, we can control the appearance of MR or its configuration, for a particular Mach number by selecting the suitable ( $w/H$ ) ratio from the transition lines plot generated. As the extent of expansion fan interaction with the incident shock increases, the dual domain shifts its location and diminishes as a function of  $w/H$  ratio facilitating the control of the  $MR \leftrightarrow RR$  hysteresis process.

## REFERENCES

- AZEVEDO, D. J. & LIU, CHING SHI 1993 Engineering approach to the prediction of shock patterns in bounded high-speed flows. *AIAA Journal* **31** (1), 83–90, arXiv: <https://doi.org/10.2514/3.11322>.
- BAI, CHEN-YUAN & WU, ZI-NIU 2017 Size and shape of shock waves and slipline for mach reflection in steady flow. *Journal of Fluid Mechanics* **818**, 116–140.
- CLARKE, JF 2002 Handbook of shock waves, volumes 1, 2, and 3. edited by g. ben-dor, o. igra & t. elperin. academic, 2001. 889, 792 and 421 pp. isbn 012 086430 4. *Journal of Fluid Mechanics* **453**, 439–443.
- GLASS, I. I. 1991 Over forty years of continuous research at utias on nonstationary flows and shock waves. *Shock Waves* **1** (1), 75–86.
- HILLIER, R. 2007 Shock-wave/expansion-wave interactions and the transition between regular and mach reflection. *Journal of Fluid Mechanics* **575**, 399–424.
- LI, H. & BEN-DOR, G. 1996 Oblique-shock/expansion-fan interaction - analytical solution. *AIAA Journal* **34** (2), 418–421, arXiv: <https://doi.org/10.2514/3.13081>.

- LI, H. & BEN-DOR, G. 1997 A parametric study of mach reflection in steady flows. *Journal of Fluid Mechanics* **341**, 101–125.
- MOUTON, CHRISTOPHER A. & HORNUNG, HANS G. 2007 Mach stem height and growth rate predictions. *AIAA Journal* **45** (8), 1977–1987, arXiv: <https://doi.org/10.2514/1.27460>.
- NEL, LARA, SKEWS, BERIC & NAIDOO, KAVENDRA 2015 Schlieren techniques for the visualization of an expansion fan/shock wave interaction. *Journal of Visualization* **18** (3), 469–479.
- YAO, Y., LI, S. G. & WU, Z. N. 2013 Shock reflection in the presence of an upstream expansion wave and a downstream shock wave. *Journal of Fluid Mechanics* **735**, 61–90.